vulcanhammer.net
July 2019

DOI: 10.13140/RG.2.2.22311.09125/1

Application of the STADYN Program to Analyze Piles Driven Into Sand

Don C. Warrington
University of Tennessee at Chattanooga
Department of Mechanical Engineering

The STADYN program was developed for the analysis of driven piles both during installation and in axial loading. Up until now the test cases used were in predominantly cohesive soils. In this paper, the expansion of the program's use into predominantly cohesionless stratigraphies has required consideration of two important factors. The first is the difference between strain-softening in clays as opposed to sands, and additionally static vs. dynamic strain effects. This requires a review of the whole concept of the "magical radius" for pile elasticity. The second is the effect of dilatancy on the response of the pile to axial loading. Both of these are discussed in this paper, and test cases are presented to illustrate the application of the program to actual driven piles.

Keywords: STADYN, pile dynamics, static load testing, magical radius, soil shear modulus, strain softening

Introduction

With the publication of Warrington (2019), the ability of the STADYN program to analyze piles driven into predominantly cohesive soils was enhanced with the quantification of the effects of strain-softening. The next step in the development of the program is its extension into predominantly cohesionless soils. Although the selection of the Mohr-Coulomb model in Warrington (2016) was an important prerequisite to facilitate this transition, two major aspects of the program needed to be addressed.

The first is whether strain-softening is substantially different in sands than clays. The effect on grain size on the small-strain shear modulus is outlined in Warrington (2019), but it is reasonable to assume that the subsequent strain-softening effects are different between the two soil types (and those in between.) This in turn requires that two other topics be addressed: whether the static and dynamic softening is singficantly different, and the matter of the "magical radius" and "magical distance" for the pile shaft and toe respectively. As shown by Warrington (2019), the magical radius and distance are application-specific parameters which affect the relationship of the strain-softening characteristics of the soil to the reduction in the stiffness of the soil-pile interface. The interrelation of these topics, combined with the state of the data in the literature, made sorting out the issues involved complex, but such sorting out is necessary to come to a reasonable understanding of the elastic response of the soil to loading, static or dynamic.

The second is the effect of dilatancy on the response of the granular soils surrounding the piles to loading. Dilatancy was discussed in Warrington (2016) and it was shown that increasing the dilitancy angle increased the capacity of the pile. While conservatism is important for routines such as STADYN, its accuracy can be significantly impaired by the omission of an important parameter, and so the proper quantification of that parameter must be considered.

Variations in Strain-Softening Response of Soils

The improvements in the STADYN program described by Warrington (2019) depended upon the static strain-softening response described by Vardanega and Bolton (2013). A plot of this is shown in 1.

The equation for this curve is

$$\mu = \frac{1}{1 + \gamma'^{0.736}} \tag{1}$$

While most of the strain-softening curves in the literature "look" like that shown in 1, they may or may not be the same. The problem begins with Vardanega and Bolton (2013) because, in addition to the difference between the reference strains for static and dynamic response, the dynamic exponent of γ' is different than the static one. Moreover other formulations of this curve have a different value of μ when the soil strain equals the reference strain, a phenomenon which will be discussed shortly. To begin the analysis, the relationship of Equation (1) should be generalized to

This paper is dedicated to the memory of Richard "Dick" Nelson, one of the founders of Pile Equipment in Jacksonville, FL. He helped me obtain Kett and McDaniel (1987) and among others kindled my interest in pile dynamics. He is still missed.

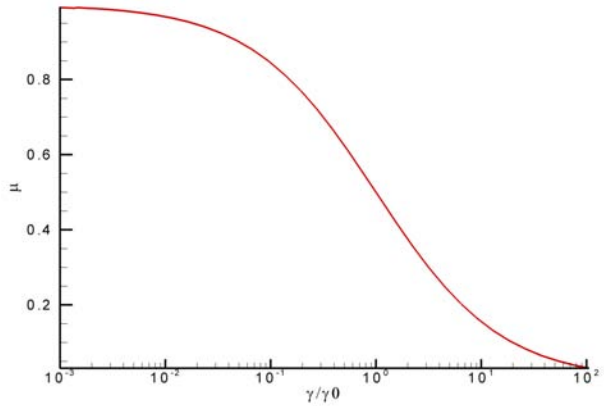

Figure 1. Softening Coefficient vs. Normalized Shear Strain (adapted from Vardanega and Bolton (2013))

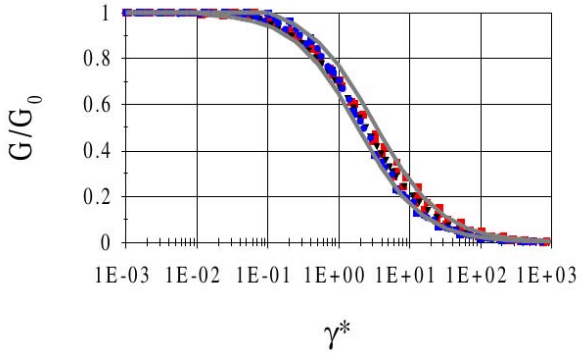

Figure 2. Upper and Lower Bound Strain Softening Coefficients (from Santos and Correia (2000))

$$\mu = \frac{\beta}{\beta + \gamma'^{\alpha}} \tag{2}$$

The strain softening coefficient at the reference strain is defined as μ_0, at which point $\gamma' = 1$. For any value of α,

$$\beta = \frac{1}{\frac{1}{\mu_0} - 1} \tag{3}$$

which is obviously undefined at the extremes of μ_0, i.e. $\mu_0 = 0$ or $\mu_0 = 1$. Vardanega and Bolton (2013) consistently define the reference strain at the point where $\mu_0 = 0.5$, thus $\beta = 1$. However, the values of α they statistically arrive at from their literature search differ between static and dynamic conditions. For the former $\alpha = 0.736$; for the latter, $\alpha = 0.943$. This change is potentially significant.

A more serious consideration, however, is that of Santos and Correia (2000). They reduced data taken from Vucetic and Dobry (1991) and Ishibashi and Zhang (1993) and were able, like Vardanega and Bolton (2013), to produce an upper and lower bound unified softening curve by applying a reference strain. This is important because the range of soils studied by Santos and Correia (2000) includes soils with a wide variety of plasticity indices, which means that they apply to the sands into which STADYN is being extended. The result of this is shown in Figure 2, where the two gray lines are the upper and lower bound curves, $\mu = \frac{G}{G_o}$ and $\gamma* = \gamma'$.

The upper and lower bound curves are fairly close; if their average is taken, the result can be expressed in terms of Equation (2) if $\alpha = 1$ and $\beta = \frac{7}{3}$. It is also evident that, for this correlation, $\mu_0 = 0.7$.

The principal difference between the two correlations is the definition of reference strain. Vucetic (1994) defines the reference strain in terms of a three-stage progressive failure of the soil. Vardanega and Bolton (2013) define it in terms of the ratio of the failure shear stress to the small-strain shear modulus. The definition of Vardanega and Bolton (2013) is central in Warrington (2019) to the elastic deflection of driven piles.

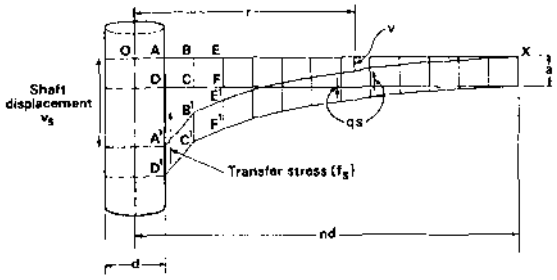

Figure 3. Pile Shaft Soil Segments and Deflection (from Cooke (1974))

These variations certainly complicate any application of strain softening to a broader variety of soils. At this point the best way to move forward is to simply analyze the effect of changing both α and β on the deflection, which should allow the identification of the crucial parameters. To do this requires a re-examination of the whole concept of the "magical radius" and "magical distance," which is the next topic.

Revisiting the "Magical Radius"

The first use of the term "magical radius" can be attributed to Randolph and Wroth (1978), although the concept was present in Cooke (1974) and Frank (1975). The model they all adopted for the shaft resistance assumed an elastic continuum around the pile shaft. Vertical effects are ignored; the problem is assumed to be plain strain in plan view (Frank (1975).) The area around the pile is divided up into annular differential elements, as shown in Figure 3.

Applying elastic theory and static equilibrium, it is possible to estimate the deflection of the soil from the pile surface outwards. If the shear modulus is assumed constant, the deflection at the shaft can be computed by the equation

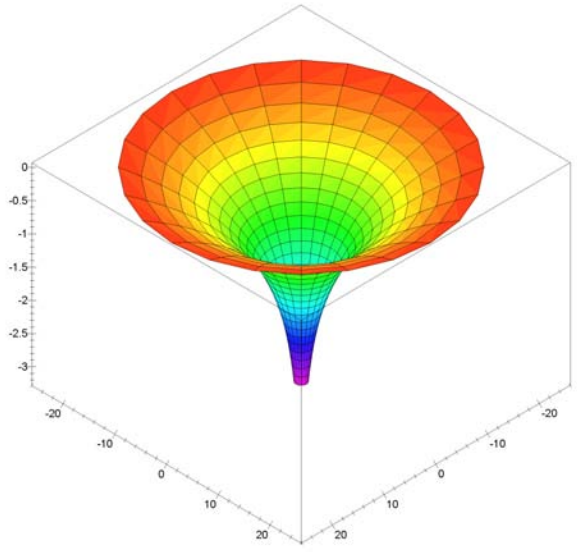

Figure 4. Dimensionless Elastic Soil Deflection Around the Pile Shaft, $r_{rat} = 25$

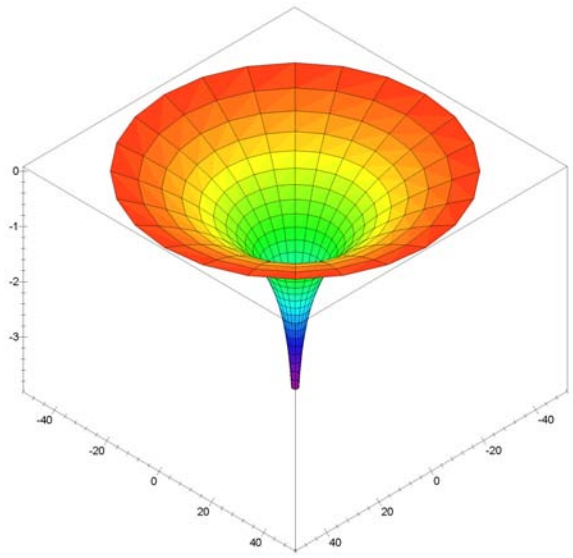

Figure 5. Dimensionless Elastic Soil Deflection Around the Pile Shaft, $r_{rat} = 50$

$$w_s = \frac{\tau_0 r_0}{G} \ln\left(\frac{r_m}{r_0}\right) \tag{4}$$

Warrington (2019) shows that this can be reduced to the dimensionless formulation

$$\bar{w_s} = \frac{1}{\mu} \ln\left(r_{rat}\right) \tag{5}$$

In principle the effects of elasticity extend to an infinite distance from the pile; however, Equation (5) shows that, as $r_{rat} \to \infty$, $\bar{w_s} \to \infty$. Thus it is necessary to limit r_{rat}, and the maximum value of r_m is referred to as the "magical radius."

To illustrate the effects of varying the magical radius, three-dimensional representations of the dimensionless deflection from the pile surface outwards are shown in Figures 4, 5 and 6 for values of $r_{rat} = 25$, 50, & 100 respectively, all assuming $\mu = 1$.

Figure 6 can be compared with Figure 7, where a generalized softening coefficient as described by Warrington (2019) is applied. The greater deflection due to the softening of the soil is noted.

It can be seen that, as the magical radius increases, the slope of the deflection around the outside rim likewise decreases. That slope is, of course, the strain of the soil at the magical radius. An ostensibly simple way of defining the magical radius would be to define a strain at which point further soil strain is negligible. Complicating this is the fact that, according to Frank (1975), the magical radius is influenced by the effects of cavity expansion in the soil.

At this point, probably the best estimate for the magical

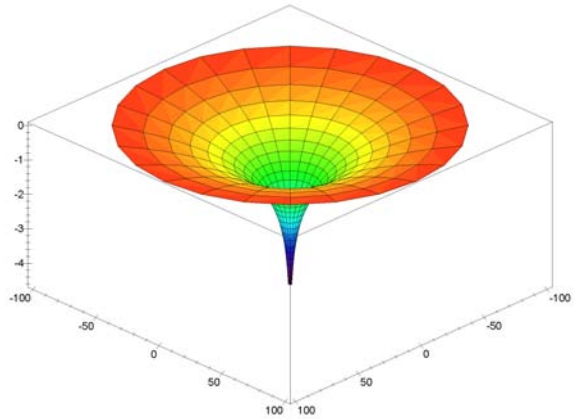

Figure 6. Dimensionless Elastic Soil Deflection Around the Pile Shaft, $r_{rat} = 100$

radius is the formula (Randolph and Wroth (1978); Warrington (2019)) is

$$r_{rat} = 2\left(\frac{L_p}{D}\right)(1 - \nu) \tag{6}$$

Using this formulation actually brings the magical radius more in line with the experimentally observed values of Salgado, Loukidis, Abou-Jaoude, and Zhang (2015). If a range of length to diameter ratios for the pile and general values of Poisson's Ratio are applied to Equation (6), the result can be seen in Figure 8.

The values of Poisson's Ratio (nu on the plot) are varied between a typical value for cohesive soils $\left(\nu = \frac{1}{2}\right)$ and cohe-

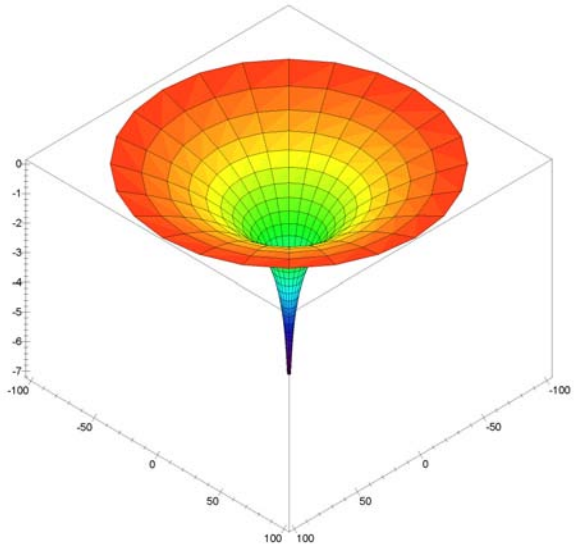

Figure 7. Dimensionless Elastic Soil Deflection Around the Pile Shaft, $r_{rat} = 100$, $\mu = 0.65$

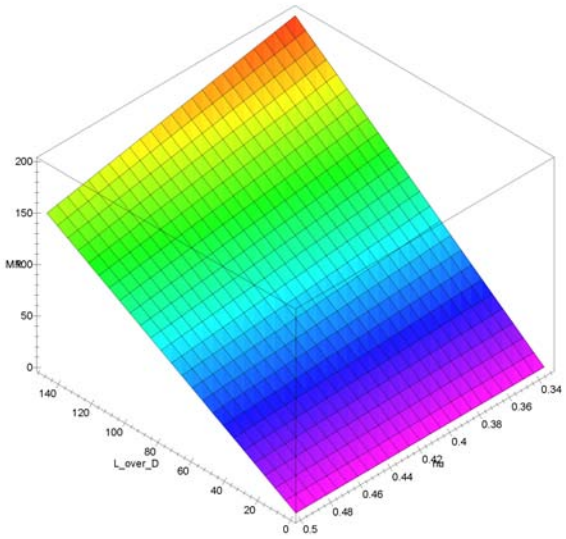

Figure 8. Magical Radius Variation

sionless ones $\left(\nu = \frac{1}{3}\right)$. It shows that, for many typical driven piles, the range of magical radius (vertical axis) does not exceed 100. Thus the range represented in Figures 4, 5 , 6 and 7 is a reasonable one.

At this point a variation of the α and β variables in Equation (2) to determine equivalent μ values is appropriate. The six cases and the figure numbers for the results are shown in Table (1). The method used to generate these plots was described in Warrington (2019), although the equation for the normalized strain is generalized to

Table 1
Figures for Equivalent μ Values

L/D	Sand $\left(\nu = \frac{1}{3}\right)$	Clay $\left(\nu = \frac{1}{2}\right)$
25	Figure 9	Figure 12
50	Figure 10	Figure 13
100	Figure 11	Figure 14

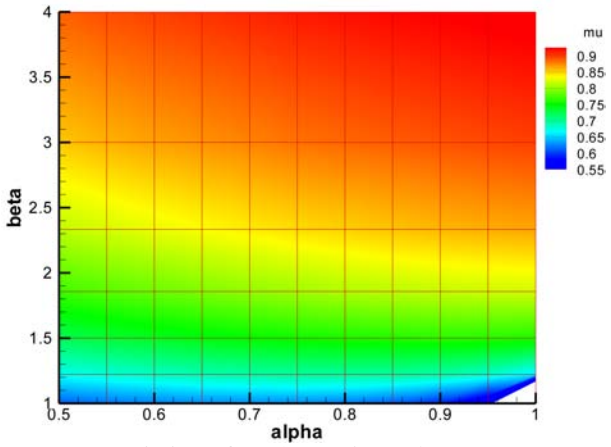

Figure 9. Variation of μ, $L/D = 25$, Sand

$$\gamma' r_{rat} = \frac{\beta + \gamma'^{\alpha}}{\beta} \tag{7}$$

The following can be seen from these figures:

1. There is a singularity where $\alpha = \beta = 1$ because the derivative of Equation (7) is undefined. This is not that significant of a problem because of the practical ranges of α avoid this point.

2. The variations in μ as a function of α do not seem to be very significant at $\beta = 1$. Those variations are more important as β increases but may not be significant due to the nature of the analysis.

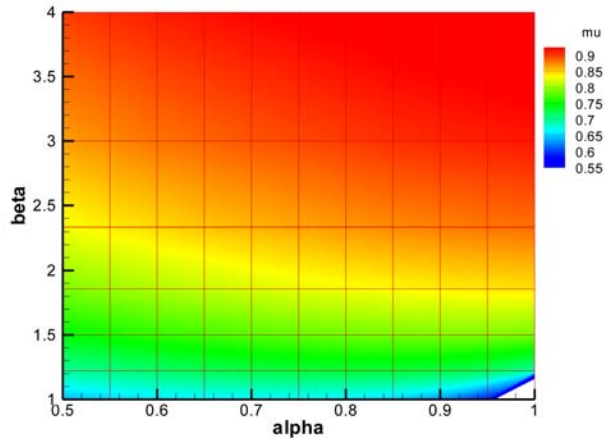

Figure 10. Variation of μ, $L/D = 50$, Sand

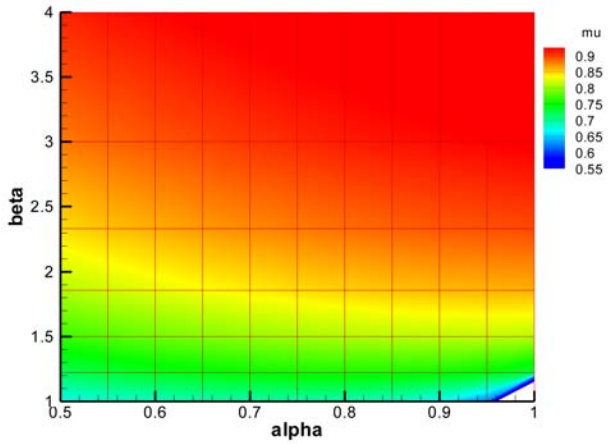

Figure 11. Variation of μ, $L/D = 100$, Sand

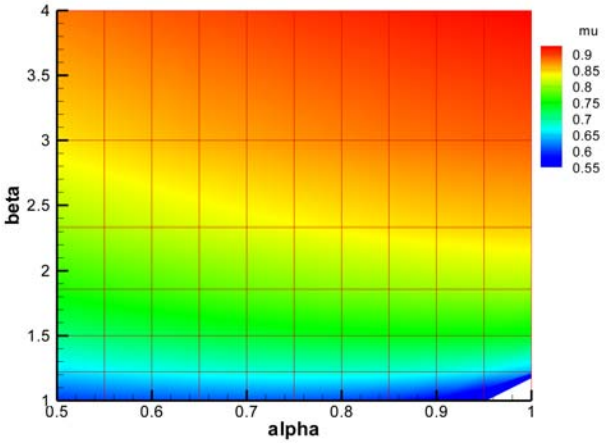

Figure 12. Variation of μ, $L/D = 25$, Clay

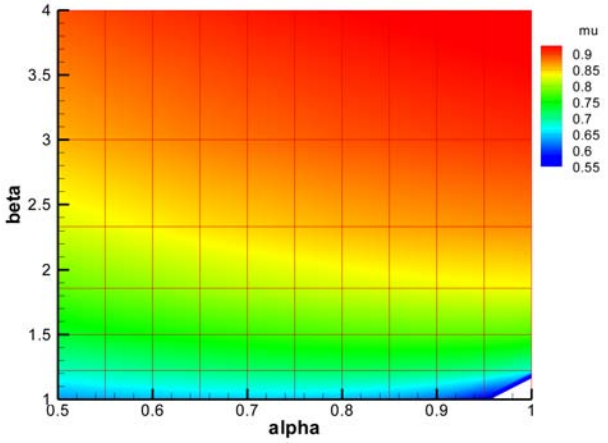

Figure 13. Variation of μ, $L/D = 50$, Clay

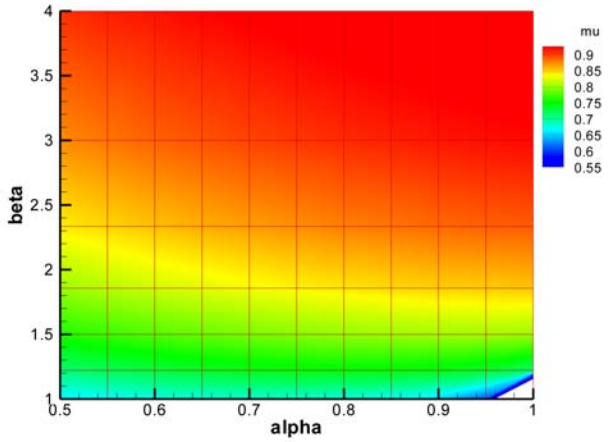

Figure 14. Variation of μ, $L/D = 100$, Clay

3. The results are reasonably consistent with variations in magical radius.

4. The value of μ consistently and significantly increases with β.

The last point brings back consideration of the reference strain vs. μ. Definition and selection of the reference strain is important to determining the equivalent softening coefficient. Equation (3) shows that the value of β is related to the softening coefficient at the reference strain. The two models presented in this paper represent differing failure concepts.

For the purposes of STADYN, the definition of reference strain given in Vardanega and Bolton (2013) (and thus $\beta = 1$) will be used because STADYN's model is an elasto-plastic model, which assumes a definite, singular failure surface for the soil. The model of Vucetic (1994) assumes a three-stage failure process, which would require a soil model more complex than STADYN's to properly replicate its failure. The use of a Mohr-Coulomb elastic-perfectly plastic model for STADYN has limitations which were understood from its inception (Warrington (2016).)

This decision having been made, a closer examination of the variations of α for the case of $\beta = 1$ is in order, and is shown in Figure 15 for sand and Figure 16 for clay.

These results show that, within limits and for a wide range of α, the equivalent softening coefficient values fall within a fairly narrow range of values, given the limitations of the model. If the static vs. dynamic values of α from Vardanega and Bolton (2013) are compared, the dynamic response of the soil is a little softer than the static one. The assumption that the static and dynamic response of the soil due to strain are at least similar is an important one for dynamic pile testing and wave equation analysis, and although this comparison is certainly neither definitive nor comprehensive it is helpful.

Given these results, for the immediate future the shaft generalized softening coefficient of $\mu = 0.65$ as derived by War-

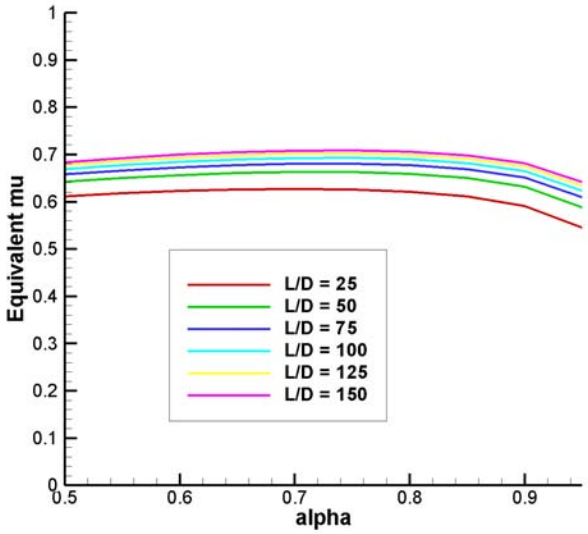

Figure 15. Variation of $\mu, \beta = 1$, Sand

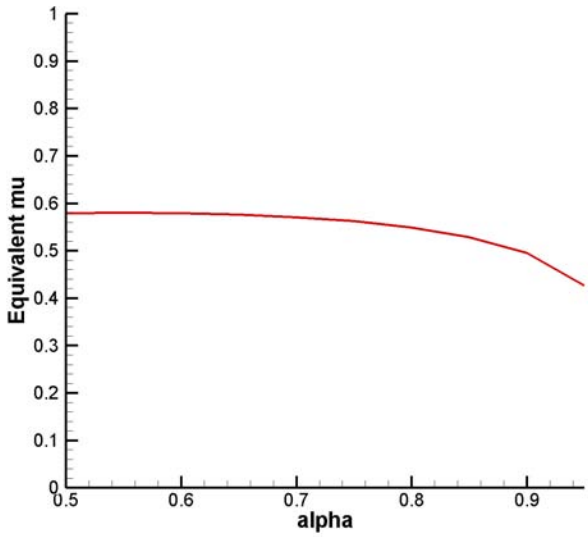

Figure 17. Toe Variation of $\mu, \beta = 1$, Sand

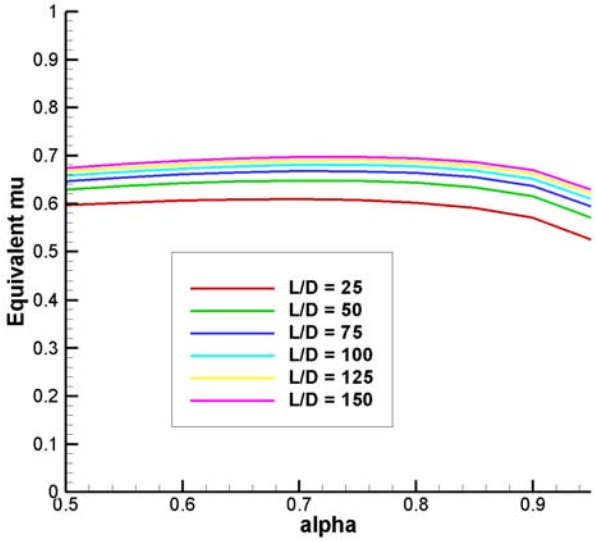

Figure 16. Variation of $\mu, \beta = 1$, Clay

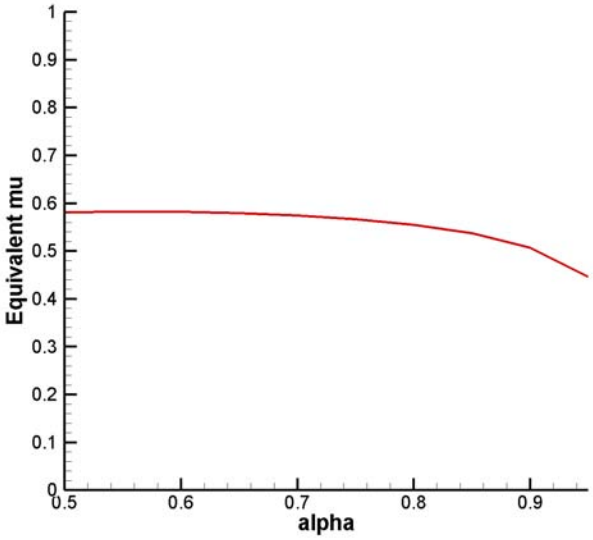

Figure 18. Toe Variation of $\mu, \beta = 1$, Clay

rington (2019) will be maintained.

Considering the "Magical Distance"

The equivalent softening coefficient at the toe can be computed in a similar fashion to that of the shaft, as shown by Warrington (2019). Defining a "magical distance" analogously to the "magical radius" is not as well documented; moreover, in an elastic medium the stresses and strains at the toe fall of more quickly than they do around the shaft, and thus a value for the equivalent softening coefficient will converge more quickly. Based on the work of Warrington (2019), a ratio of distance from the toe to the toe radius of 100 will be used to determine the effects of α on the softening coefficient. This is shown in Figures 17 and 18.

The trends are very similar to those of the shaft; however, the values of μ indicated are lower. Based on these results, the value of $\mu = 0.55$ will be set for the toe resistance.

Effects of Dilatancy

Early trials with a predominantly cohesionless soil profile resulted in low capacity predictions. The extensive work on the elastic response of the soil embodied in this paper and Warrington (2019) was in part a response to this result. The difficulties with the elastic response resolved, continued problems indicated that another factor was at work. A likely reason for this was the neglect of dilatant effects.

Dilitant effects on driven piles in cohesionless soils were a centerpiece of Frank (1975), who used a dilatancy model

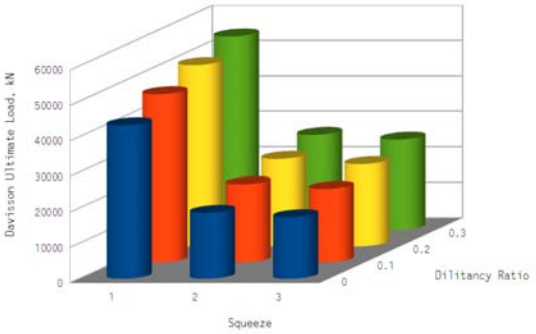

Figure 19. Effect of Lateral Squeeze and Dilatancy Ratio of Pile Capacity (from Warrington (2016))

which is different from that of Warrington (2016). The latter included a study on the effect of dilatancy on static pile capacity; a summary of those results is in Figure 19, which was combined with a study of lateral element squeeze.

It is evident that pile capacity increases with dilatancy. Quantifying that dilitancy, however, is not a straightforward matter. Cinicioglu and Abadkon (2015) established a relationship between dilitancy, relative density and mean effective stress of the form

$$\psi = tan^{-1}\left(\hat{\alpha}\left(\frac{\sigma_0}{p_{atm}}\right) + m_\psi D_r\right) \tag{8}$$

The first term is the relationship of the dilatancy angle to the mean effective stress. As the mean effective stress increases, the ability of the soil to undergo volume change (a central characteristic of dilitant soils) as the confining stress increases, thus $\hat{\alpha}$ is negative. The second term relates the dilatancy to the relative density and (by extension in STADYN's system of soil parameters) the dry density, and thus m_ψ is positive.

Cinicioglu and Abadkon (2015) performed tests on sands from the Silivri district west of Istanbul, Turkey. They established values of $\hat{\alpha} = -0.06$ and $m_\psi = 0.35$ for these soils. They also performed a literature search to verify the form of Equation (8). Analyzing the result of the data they collected indicated a mean $\hat{\alpha} = -0.043$ and $m_\psi = 0.56$ with a standard deviation of 0.039 and 0.281 for each result. This underscores the wide scatter in the results and the need to test a given soil individually for its properties.

They also noted that there are other forms to estimate the dilatancy angle. The correlation they cited involves the use of the critical friction angle. Although this quantity is very important and additionally is an important component in critical state soil mechanics, it generally does not involve a property that is commonly tested in soils.

STADYN generally considers the dilatancy angle as a function of the internal friction angle, thus

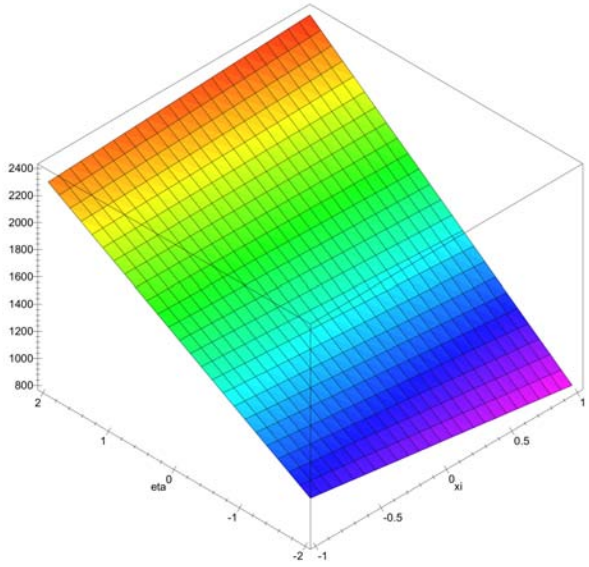

Figure 20. Dry density in $^{kN}/_{m^3}$ as a function of ξ and η

$$\psi = r_{dil}\phi \tag{9}$$

which is illustrated in Figure 19. This is because, in the $\xi - \eta$ system that STADYN uses for soil properties, as soils transition away from purely cohesionless ones ($\xi = -1$,) they become less cohesionless and thus the internal friction angle is reduced. It is reasonable to assume that, under these conditions, they become less dilatant, as they approach a purely cohesive state where $\phi = \psi = 0$. For each soil layer STADYN computes both the effective stress and the mean effective stress, the latter using the lateral earth pressure coefficient computed via Poisson's Ratio. The relative density is simple to compute for soils where $\xi = -1$: $D_r = 0$ when $\eta = -1$ and $D_r = 100\%$ when $\eta = 1$, and other values by linear interpolation.

Adjustments of Soil Properties

The transition to analyzing cohesionless stratigraphies led to a couple of adjustments in the soil properties that STADYN uses to construct its layering system

The first was a small increase in the minimum dry density for purely cohesionless soils ($\xi = \eta = -1$) from $1200^{kN}/_{m^3}$ to $1400^{kN}/_{m^3}$. This brings it more into line with standard tabulations of soil properties. The variation in dry density as a function of ξ and η is shown in Figure 20.

An interesting plot is the plot of small-strain ($\mu = 1$) modulus of elasticity as a function of the same two variables, shown in Figure 21.

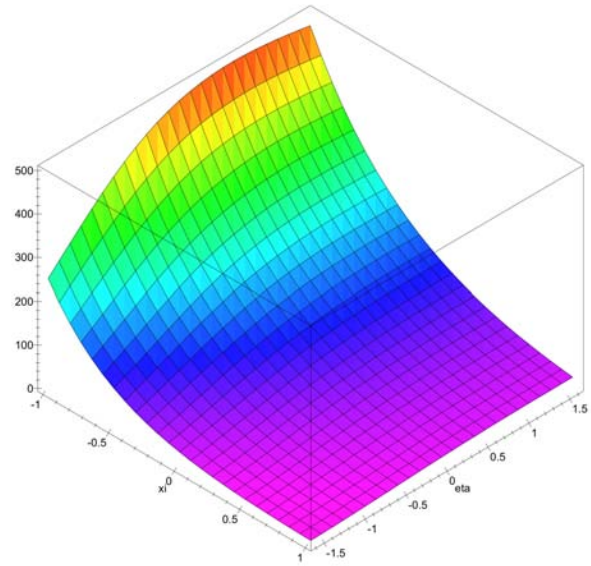

Figure 21. Small-strain ($\mu = 1$)elastic modulus in *MPa* as a function of ξ and η

Comparison with Static Load Test Data in Cohesionless Stratigraphies

The last part will concern itself with how STADYN performs with load test data for concrete piles driven into predominantly cohesionless stratigraphies. The source of the data here will be Kett and McDaniel (1987). It was chosen because all of the test cases discussed were in predominantly cohesionless soils; the location of the various sites examined are shown in Figure 22. Additionally complete soil boring data, driving logs and CAPWAP results were available for these cases.

Three cases from this study were considered: Site 1A, 3B and 4A. Summaries for each case are given in Figures 23, 24 and 25 respectively.

The cases were set up in the usual way except that only Case 3B had a dynamic analysis with a Vulcan 510 hammer; the other two had static load tests only. Initially these cases were set up with no dilitancy; however, the Davisson capacities returned by STADYN were considerably lower than the actual static load test results. After this dilitancy was added in the range of the average from Cinicioglu and Abadkon (2015) and also the results of the Silivri tests using Equation (8). In both cases the resulting capacities were much higher. Finally the value of m_ψ was set at 0.10 and, along with $\alpha = -0.06$, more satisfactory results were obtained, especially for Cases 1A and 3B. This is evident by the static load comparisons of Figures 26 and 27.

The results of Case 1A are probably the best seen to date with STADYN and static load tests. The Case 3B result is the opposite of what was obtained in the Finno (1989) case (Warrington (2019)) in that the static load test results showed

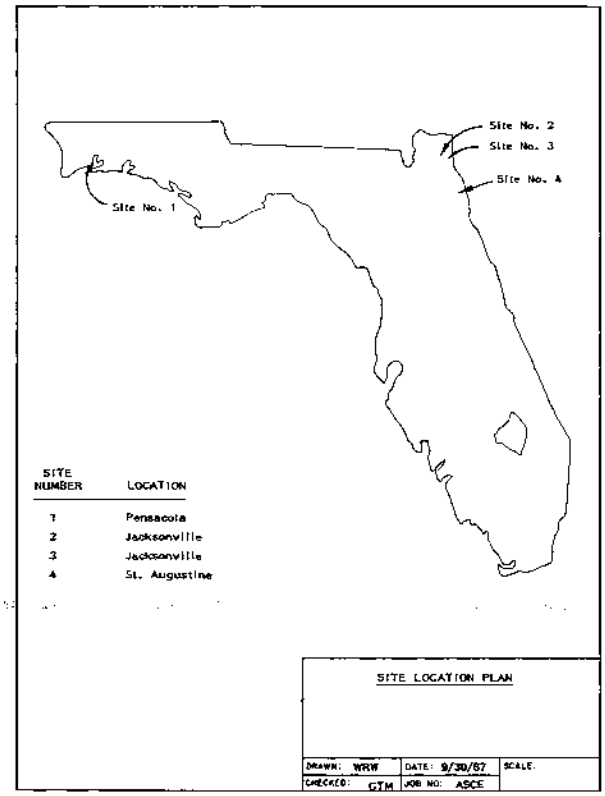

Figure 22. Locations of cases from Kett and McDaniel (1987)

Table 2
Summary of Results for Cases from Kett and McDaniel (1987)

Case	Davisson Capacity, kN		
	Static Load Test	STADYN, no dilatancy	STADYN, with dilatancy
1A	2756	2240	2710
3B	2560	1410	2590
4A, $m_\psi = 0.10$	596	323	521
4A, $m_\psi = 0.15$			604

a stiffer response to load than STADYN predicted. In both cases the Davisson capacities were very close.

A less satisfactory result was obtained for Case 4A using $m_\psi = 0.10$, as shown in Figure 28, where STADYN underpredicted the Davisson capacity. Better results were obtained when m_ψ was increased to 0.15, as shown in Figure 29. A tabular result of these test cases is shown in Table 2.

Discussion

1. Generalizing the strain-softening relationship into Equation (2) highlights the matter of the relationship between the reference strain and the ratio of the shear modulus at that reference strain to the small strain modulus. While differing failure definitions and models are understandable with

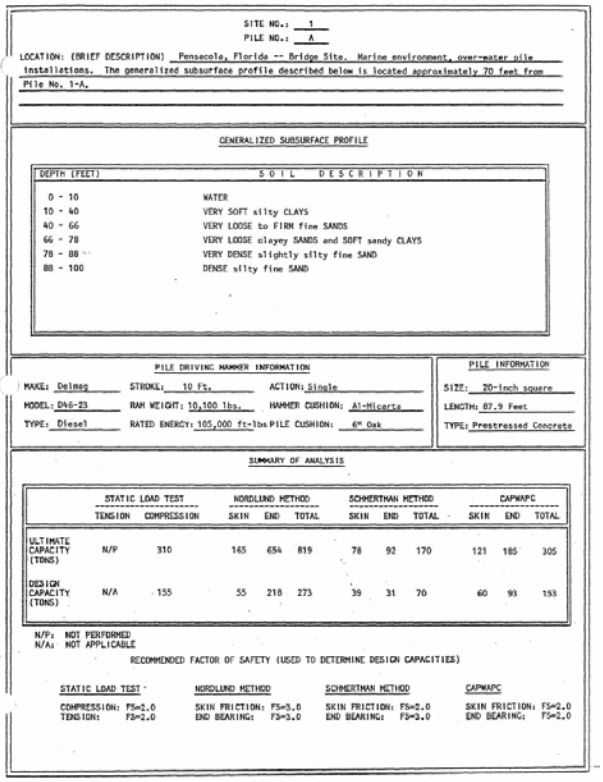

SITE NO.: 1
PILE NO.: A

LOCATION: (BRIEF DESCRIPTION) Pensacola, Florida -- Bridge Site. Marine environment, over-water pile installations. The generalized subsurface profile described below is located approximately 70 feet from Pile No. 1-A.

GENERALIZED SUBSURFACE PROFILE

DEPTH (FEET)	SOIL DESCRIPTION
0 - 10	WATER
10 - 40	VERY SOFT silty CLAYS
40 - 66	VERY LOOSE to FIRM fine SANDS
66 - 78	VERY LOOSE clayey SANDS and SOFT sandy CLAYS
78 - 88	VERY DENSE slightly silty fine SAND
88 - 100	DENSE silty fine SAND

PILE DRIVING HAMMER INFORMATION

MAKE: Delmag STROKE: 10 Ft. ACTION: Single
MODEL: D46-23 RAM WEIGHT: 10,100 lbs. HAMMER CUSHION: Al-Micarta
TYPE: Diesel RATED ENERGY: 105,000 ft-lbs PILE CUSHION: 6" Oak

PILE INFORMATION

SIZE: 20-inch square
LENGTH: 87.9 Feet
TYPE: Prestressed Concrete

SUMMARY OF ANALYSIS

	STATIC LOAD TEST		NORDLUND METHOD			SCHMERTMAN METHOD			CAPWAPC		
	TENSION	COMPRESSION	SKIN	END	TOTAL	SKIN	END	TOTAL	SKIN	END	TOTAL
ULTIMATE CAPACITY (TONS)	N/P	310	165	654	819	78	92	170	121	185	305
DESIGN CAPACITY (TONS)	N/A	155	55	218	273	39	31	70	60	93	153

N/P: NOT PERFORMED
N/A: NOT APPLICABLE

RECOMMENDED FACTOR OF SAFETY (USED TO DETERMINE DESIGN CAPACITIES)

STATIC LOAD TEST	NORDLUND METHOD	SCHMERTMAN METHOD	CAPWAPC
COMPRESSION: FS=2.0	SKIN FRICTION: FS=3.0	SKIN FRICTION: FS=2.0	SKIN FRICTION: FS=2.0
TENSION: FS=2.0	END BEARING: FS=3.0	END BEARING: FS=3.0	END BEARING: FS=2.0

Figure 23. Summary of Case 1A (from Kett and McDaniel (1987))

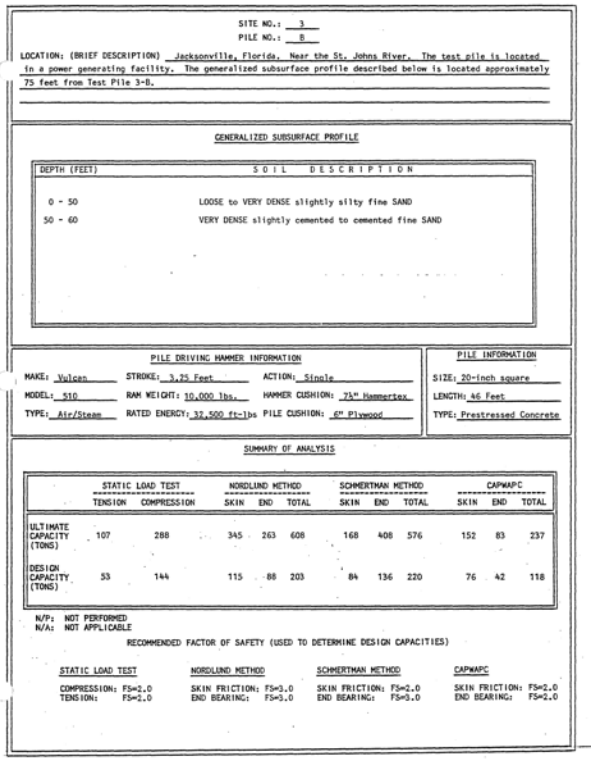

SITE NO.: 3
PILE NO.: B

LOCATION: (BRIEF DESCRIPTION) Jacksonville, Florida. Near the St. Johns River. The test pile is located in a power generating facility. The generalized subsurface profile described below is located approximately 75 feet from Test Pile 3-B.

GENERALIZED SUBSURFACE PROFILE

DEPTH (FEET)	SOIL DESCRIPTION
0 - 50	LOOSE to VERY DENSE slightly silty fine SAND
50 - 60	VERY DENSE slightly cemented to cemented fine SAND

PILE DRIVING HAMMER INFORMATION

MAKE: Vulcan STROKE: 3.25 Feet ACTION: Single
MODEL: 510 RAM WEIGHT: 10,000 lbs. HAMMER CUSHION: .75" Hammertex
TYPE: Air/Steam RATED ENERGY: 32,500 ft-lbs PILE CUSHION: 6" Plywood

PILE INFORMATION

SIZE: 20-inch square
LENGTH: 46 Feet
TYPE: Prestressed Concrete

SUMMARY OF ANALYSIS

	STATIC LOAD TEST		NORDLUND METHOD			SCHMERTMAN METHOD			CAPWAPC		
	TENSION	COMPRESSION	SKIN	END	TOTAL	SKIN	END	TOTAL	SKIN	END	TOTAL
ULTIMATE CAPACITY (TONS)	107	288	345	263	608	168	408	576	152	83	237
DESIGN CAPACITY (TONS)	53	144	115	88	203	84	136	220	76	42	118

N/P: NOT PERFORMED
N/A: NOT APPLICABLE

RECOMMENDED FACTOR OF SAFETY (USED TO DETERMINE DESIGN CAPACITIES)

STATIC LOAD TEST	NORDLUND METHOD	SCHMERTMAN METHOD	CAPWAPC
COMPRESSION: FS=2.0	SKIN FRICTION: FS=3.0	SKIN FRICTION: FS=2.0	SKIN FRICTION: FS=2.0
TENSION: FS=2.0	END BEARING: FS=3.0	END BEARING: FS=3.0	END BEARING: FS=2.0

Figure 24. Summary of Case 3B (from Kett and McDaniel (1987))

soils, such differences need to be understood in application.

2. Although the "magical radius" and "magical distance" are consequences of the application of elastic theory, quantifying them remains an elusive goal even forty years after their identification. Fortunately, for the range of practical piles and soils, the effect of varying the radius is not completely insignificant but is within a sufficiently narrow range so that it can be neglected as a factor in parameter quantification, specifically establishing a reasonable value of μ.

3. The interaction of the strain-softening relationship and the elastic continuum around the pile has also shown that the α coefficient in Equation (2) can, for the present at least, be neglected. Although the differences in static and dynamic elastic response of the soil need further quantification irrespective of the method used, their divergence can be ignored until the effects of that divergence in pile dynamics is better understood. The ability to neglect this parameter also allows application of the program in a broader range of soils without having to alter the properties used in the program.

4. Dilatant effects in cohesionless soils cannot be ignored for analyzing pile response to axial loading in these soils. Although the use of 3D finite element models is becoming more common in practice, much analysis–and indeed most dynamic analysis–of piles still utilizes 1D modeling. The dilatancy issue is one of the strongest justifications to using a 3D model for this type of analysis.

5. Even with the limited test cases analyzed here, proper quantification of the dilatancy angle remains a difficult task. The necessity of altering the m_ψ coefficient is unsurprising given the wide scatter in the data from Cinicioglu and Abadkon (2015), but doing so still begs an explanation, especially since the value used is at the lower end of that data. One possible explanation is that cavity expansion alters the confinement conditions of the soil beyond that of effective stress, an explanation suggested by the results of Frank (1975). This means that this effect is better replicated by altering the first term of Equation (8). With all of this, however, variations due to differing soil conditions cannot be discounted.

6. The dilatancy issue highlights the issue of soil properties, their quantification and application. STADYN's generalization of soil properties is always an important issue, and is a source for the variation of the results of the program from actual static or dynamic load test data. However, outside of research projects the types of soil data gathered do not permit much more precision of soil property characterization than STADYN's standard system accommodates. Put another way, it is possible to input into STADYN more detailed and specific soil properties but the data generally available does not justify this level of precision.

SITE NO.: 4
PILE NO.: A

LOCATION: (BRIEF DESCRIPTION) St. Augustine, Florida. Near the Atlantic Ocean. The test pile is located in a private school facility. The generalized subsurface profile described below is located approximately 25 feet from Test Pile 4-A.

GENERALIZED SUBSURFACE PROFILE

DEPTH (FEET)	SOIL DESCRIPTION
0 - 5	LOOSE slightly silty fine SAND
5 - 22	VERY LOOSE clayey fine SAND
22 - 32	FIRM to DENSE slightly silty fine SAND
32 - 40	FIRM to DENSE shelly fine SAND

PILE DRIVING HAMMER INFORMATION

MAKE: ICE STROKE: N/A ACTION: Double
MODEL: 440 RAM WEIGHT: 4000 lbs. HAMMER CUSHION: 2¾" Al. & Micarta
TYPE: Diesel RATED ENERGY: 19,840 ft-lbs PILE CUSHION: 4¾" Pinewood

PILE INFORMATION

SIZE: 12-inch square
LENGTH: 28 Feet
TYPE: Prestressed Concrete

SUMMARY OF ANALYSIS

	STATIC LOAD TEST		NORDLUND METHOD			SCHMERTMAN METHOD			CAPWAPC		
	TENSION	COMPRESSION	SKIN	END	TOTAL	SKIN	END	TOTAL	SKIN	END	TOTAL
ULTIMATE CAPACITY (TONS)	N/P	67	13	65	78	24	96	120	N/P	N/P	N/P
DESIGN CAPACITY (TONS)	N/A	33	4	22	26	12	32	44	N/A	N/A	N/A

N/P: NOT PERFORMED
N/A: NOT APPLICABLE

RECOMMENDED FACTOR OF SAFETY (USED TO DETERMINE DESIGN CAPACITIES)

STATIC LOAD TEST	NORDLUND METHOD	SCHMERTMAN METHOD	CAPWAPC
COMPRESSION: FS=2.0	SKIN FRICTION: FS=3.0	SKIN FRICTION: FS=2.0	SKIN FRICTION: FS=2.0
TENSION: FS=2.0	END BEARING: FS=3.0	END BEARING: FS=3.0	END BEARING: FS=2.0

Figure 25. Summary of Case 4A (from Kett and McDaniel (1987))

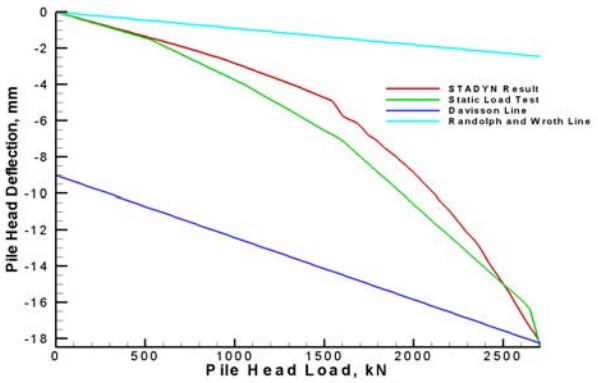

Figure 26. Load test results for Case 1A

Conclusion

The extension of the STADYN program into the analysis of piles driven into predominantly cohesionless soils has required an extensive investigation of both elastic and dilatant properties of soils. That investigation has resulted in modifications to the program which broaden its use. That broadening is not without qualification and the need for further study and the application of more field data (specifically static load test data) but at this point STADYN's development has reached a point where acquisition of such data can result in significant progress both for the program and pile dynamics.

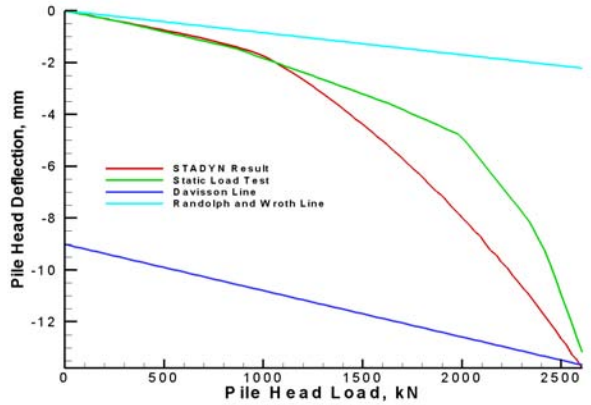

Figure 27. Load test results for Case 3B

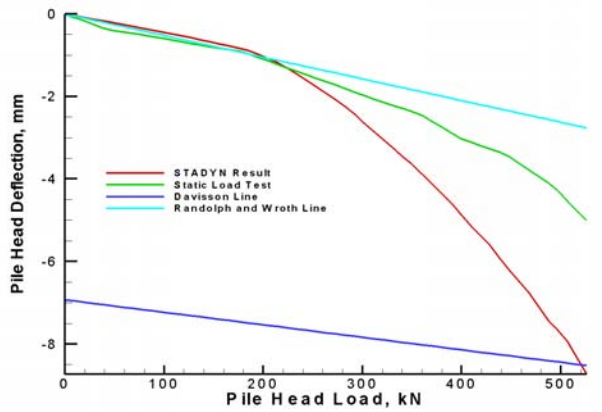

Figure 28. Load test results for Case 4A, $m_\psi = 0.10$

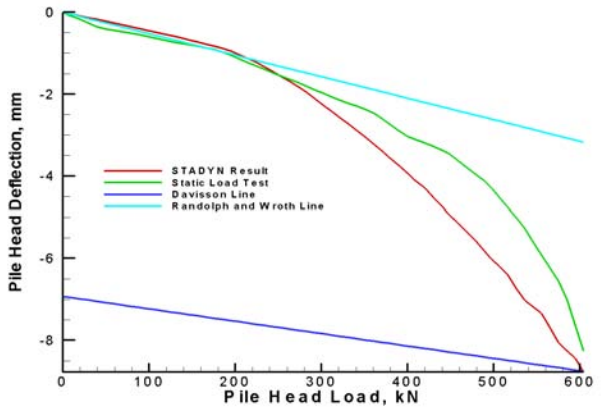

Figure 29. Load test results for Case 4A, $m_\psi = 0.15$

Nomenclature

α	Parameter for strain-softening coefficient
β	Parameter for strain-softening coefficient
$\hat{\alpha}$	Dilatancy coefficient for effective stress
μ_0	Strain-softening coefficient at the reference strain
ϕ	Internal friction angle, degrees
ψ	Dilatancy angle, degrees
σ_0	Mean effective or deviatoric stress, kPa
D_r	Relative density, decimal (not percent)
m_ψ	Dilatancy coefficient for relative density
p_{atm}	Atmospheric pressure, kPa
r_{dil}	Dilatancy ratio
$\bar{w_s}$	Normalized Pile Displacement
γ	Shear Strain
γ', $\gamma*$	Ratio of soil shear strain to reference strain
γ'	Normalized Shear Strain
μ	Hyperbolic strain softening coefficient
ν	Poisson's Ratio
τ_0	Shear Stress at Pile Shaft Interface, kPa
ξ, η	Dimensionless Soil Coefficients for STADYN
D	Diameter of pile, m
G	Shear Modulus of Elasticity, kPa
G_0	Small-Strain Shear Modulus of Elasticity, kPa
L_p	Length of pile, m
r	Radius From Pile Center, m
r_0	Pile Outside Radius, m
r_m	Magical Radius, m
r_{rat}	Magical Radius ratio
w_s	Deflection at Pile Surface, m

References

Cinicioglu, O., & Abadkon, A. (2015, April). Dilatancy and friction angles based on in situ soil conditions. *Journal of Geotechnical and Geoenvironmental Engineering*, *141*(4), 06014019–1–7. doi: 10.1061/(ASCE)GT.1943-5606.0001272

Cooke, R. (1974, December). The settlement of friction pile foundations. *Conference on Tall Buildings, Peninsular Malaysia Conference Organizing Committee*, 7–19.

Finno, R. (1989). *Predicted and observed axial behavior of piles: Results of a pile prediction symposium*. New York, NY: American Society of Civil Engineers.

Frank, R. (1975). *Etude theorétique du comportement des pieux sous charge verticale introduction de la dilatance* (Unpublished doctoral dissertation). Laboratoire Central des Ponts et Chausées.

Ishibashi, I., & Zhang, X. (1993). Unified dynamic shear moduli and damping ratios of sand and clay. *Soils and Foundations*, *33*(1), 182–191. doi: 10.3208/sandf1972.33.182

Kett, K. F., & McDaniel, G. T. (1987, August). Methods for prediction of the ultimate tension and compression capacities of prestressed concrete piles in fine sands. *Annual Meeting, Florida Section, American Society of Civil Engineers*.

Randolph, M., & Wroth, C. (1978, December). Analysis of deformation of vertically loaded piles. *Journal of the Geotechnical Engineering Division*, *104*(GT12).

Salgado, R., Loukidis, D., Abou-Jaoude, G., & Zhang, Y. (2015). The role of stil stiffness non-linearity in 1d pile driving simulations. *Geotechnique*, *65*(3), 169–187.

Santos, J. A. M., & Correia, A. G. (2000). Shear modulus of soils under cyclic loading at small and medium strain level. In (Vol. 0530).

Vardanega, P., & Bolton, M. (2013, September). Stiffness of clays and silts: Normalizing shear modulus and shear strain. *Journal of Geotechnical and Geoenvironmental Engineerins*, *139*, 1575–1589.

Vucetic, M. (1994, December). Cyclic threshold shear strains in soils. *Journal of Geotechnical Engineering*, *120*(12), 2208-2228. doi: 10.1061/(ASCE)0733-9410(1994)120:12(2208)

Vucetic, M., & Dobry, R. (1991, January). Effect of soil plasticity on cyclic response. *Journal of Geotechnical Engineering*, *117*(1), 87–107.

Warrington, D. C. (2016). *Improved methods for forward and inverse solution of the wave equation for piles* (Unpublished doctoral dissertation). University of Tennessee at Chattanooga, Chattanooga, TN.

Warrington, D. C. (2019, April). Effective hyperbolic strain-softened shear modulus for driven piles in clay. *University of Tennessee at Chattanooga*, *2019 Research Dialogues*. doi: 10.13140/RG.2.2.14305.15205